A Parameterized Macromodeling Strategy with Uniform Stability Test

A Parameterized Macromodeling Strategy With Uniform Stability Test

Piero Triverio, *Student Member, IEEE*, Stefano Grivet-Talocia, *Senior Member, IEEE*, and Michel S. Nakhla, *Fellow, IEEE*

***Abstract*—This paper presents a strategy for the construction of parameterized linear macromodels from tabulated port responses. These macromodels are able to reproduce the input-output behavior of the structure of interest both in terms of frequency and one or more design variables such as geometry and material parameters. A highly efficient combination of rational identification and piecewise linear interpolation leads to a macromodel form which can be cast as a polytopic descriptor form. This in turns enables the construction of a numerically robust testing procedure, based on linear matrix inequalities, for the assessment of uniform model stability within any prescribed region of the parameters space. Several numerical examples are used to illustrate the theory on practical application cases.**

***Index Terms*—Descriptor forms, linear macromodeling, parameterization, polytopes, scattering, stability.**

I. Introduction and Motivations

THE COMPLEXITY of modern electronic systems calls for fully automated design and optimization workflows. In this scenario, the finalization of the physical layout of a given structure or subsystem results from lengthy optimization processes, which select the best candidate among many possible choices while maximizing some system performance metric. This optimization is usually performed by repeated system-level simulations for various combinations of the design variables.

A fundamental enabling factor for the above process is the availability of models for each structure or component. These models should be available on-demand for any configuration of the design variables, typically geometrical parameters such as interconnect width and spacing or substrate height, or material parameters such as conductivity or permittivity. Also, these models should be available in a form that is compatible with the adopted system-level solver for the evaluation of the performance metric. Circuit solvers of the SPICE class are commonly used for this task. A model with such features will be denoted as *parameterized macromodel* in the following.

Manuscript received June 17, 2008; revised September 03, 2008. First version published January 09, 2009; current version published February 13, 2009. This work was recommended for publication by Associate Editor J. Tan upon evaluation of the reviewers comments.

P. Triverio and S. Grivet-Talocia are with the Department of Electronics, Politecnico di Torino, 10129 Torino, Italy (e-mail: piero.triverio@polito.it; stefano.grivet@polito.it).

M. S. Nakhla is with the Department of Electronics, Carleton University, Ottawa, ON, K2S-5B6 Canada (e-mail: msn@doe.carleton.ca).

Color versions of one or more of the figures in this paper are available online at http://ieeexplore.ieee.org.

Digital Object Identifier 10.1109/TADVP.2008.2007913

For the nonparameterized case, a large number of results have been published over the last few years on the subject of macromodel generation/identification, addressing the stability, causality, and passivity issues (see, e.g., [1]–[18] and references therein). Macromodeling has indeed become a standard practice in various application areas. A macromodel is typically created by first running a full-wave simulation tool to extract the port responses, e.g., the frequency-dependent scattering matrix of the structure of interest. Then, suitable algorithms are applied to perform a rational approximation, possibly with passivity constraints, such that the resulting macromodel can be cast in SPICE-compatible form. Unfortunately, this process is not feasible when the structure of interest depends on one or more design variables, since the entire macromodeling flow, including the full-wave characterization step, must be repeated for each different combination of the parameters.

This paper overcomes these problems by suggesting a new parameterization scheme for linear macromodels. This approach starts from a restricted set of tabulated port responses, corresponding to few configurations of the design variables, and identifies a multivariate model that directly includes the dependence on design variables in a functional form. Parameterized modeling algorithms have been proposed for transmission line structures in [19]. For generic linear components such as connectors, vias, or passive elements, a parametric extension of the Sanathanan Koerner iteration was introduced in [20] and further improved in [21]. A similar approach, making use of orthonormal bases, was presented in [22].

There are several new contributions in this work. First, a particular functional form of the macromodel is devised (Section II), based on a combined rational frequency dependence and piecewise linear parameters dependence. A highly efficient identification process is then applied to derive the coefficients of the macromodel multivariate expression, which is valid for any continuous variation of frequency and design parameters in the range of interest (Section III). A number of state-space realizations are then constructed, leading to a parameterized polytopic descriptor form, which mimics the structure of the well-known modified nodal analysis (MNA) equations (Section IV). The availability of this form enables the construction of a parameter-independent algorithm for checking the uniform stability of the parameterized macromodel (Section V). This test is based on purely algebraic conditions, which are solved using convex optimization. Therefore, no brute-force sampling in frequency and parameters space is required. Numerical application examples (Section VI) confirm the excellent performance of the proposed technique.

II. Model Formulation

A. Problem Statement

The objective of this work is to develop a robust numerical algorithm for the generation of parameterized macromodels starting from tabulated data. The resulting models will reproduce the external ports behavior of the structure under investigation as a function of both frequency and one or more design variables, such as geometry or material parameters. The most common scenario is to derive input data samples from repeated full-wave simulations, although the main technique is applicable independently on the source of the raw structure characterization. For the sake of simplicity, the presentation of the main results will consider two design parameters only, denoted as λ and μ. All results are however valid in the most general case and for an arbitrary number of parameters, with obvious modifications.

The structure under modeling is assumed to have a linear input–output behavior, with N accessible electrical ports. Our starting point is the availability of the structure frequency responses, being known at several frequency points[1]

$$\omega \in \{\omega_k\}, \quad k = 1, \ldots, \bar{k} \tag{1}$$

and for different parameters values

$$\lambda \in \{\lambda_l\}, \quad l = 1, \ldots, \bar{l}, \tag{2}$$

$$\mu \in \{\mu_m\}, \quad m = 1, \ldots, \bar{m}. \tag{3}$$

We will denote the available data samples as

$$\mathbf{H}_{klm} \tag{4}$$

where the subscripts k, l, and m refer, respectively, to the frequency sample ω_k, and to the two parameters values λ_l and μ_m. The grid of available parameters values (λ_l, μ_m) defines a hypercube in the parameters space

$$[\lambda_1, \lambda_{\bar{l}}] \times [\mu_1, \mu_{\bar{m}}] \tag{5}$$

which provides the range of validity of the parameterized models to be constructed. In summary, we want to derive a macromodel $\mathbf{H}(s; \lambda, \mu)$ which depends continuously on frequency and parameters, and which provides the best possible approximation to the input data $\mathbf{H}_{klm}$.

B. Parameterized Model Formulation

One fundamental constraint on the functional form of the macromodel $\mathbf{H}(s; \lambda, \mu)$ is the possibility to synthesize it as a lumped circuit equivalent, so that it can be easily included in system-level simulations and optimizations using standard circuit solvers such as SPICE. This constraint calls for a rational dependence on frequency, as in most state-of-the-art linear macromodeling schemes. Rational functions can be specified in terms of poles/residues, zeros/poles, or numerator/denominator polynomials. All these formulations suffer from severe ill-conditioning when the dependence of external parameters is included [20], [21]. Therefore, we adopt the more general formulation[2]

$$\mathbf{H}(s; \lambda, \mu) = \frac{\sum_n \mathbf{R}_n(\lambda, \mu)\phi_n(s)}{\sum_n r_n(\lambda, \mu)\phi_n(s)} \tag{6}$$

where numerator and denominator are linear combinations of suitable basis functions $\{\phi_n(s)\}$. Frequency variations are induced by the basis functions, whereas parameters variations are induced by their expansion coefficients. It is straightforward to prove that (6) is a rational function of frequency whenever all basis functions are rational.

Because of very convenient numerical properties, we choose $\{\phi_n(s)\}$ to be partial fractions associated to a prescribed set of poles a_n

$$\phi_n(s) = \begin{cases} 1, & \text{for } n = 0 \\ \frac{1}{s - a_n}, & \text{for } n = 1, \ldots, \bar{n} \end{cases}. \tag{7}$$

For the expansion coefficients we adopt instead the representation

$$\mathbf{R}_n(\lambda, \mu) = \sum_{p,q} \mathbf{R}_{npq}\psi_p(\lambda)\xi_q(\mu) \tag{8a}$$

$$r_n(\lambda, \mu) = \sum_{p,q} r_{npq}\psi_p(\lambda)\xi_q(\mu) \tag{8b}$$

with the parameter-dependent basis functions $\{\psi_p(\lambda)\}$, $p = 1, \ldots, \bar{p} = \bar{l}$ being piecewise linear, given by

$$\psi_p(\lambda) = \frac{\lambda - \lambda_{p-1}}{\lambda_p - \lambda_{p-1}} I_{[\lambda_{p-1}, \lambda_p[}(\lambda) + \frac{\lambda - \lambda_{p+1}}{\lambda_p - \lambda_{p+1}} I_{[\lambda_p, \lambda_{p+1}]}(\lambda) \tag{9a}$$

for $p = 2, \ldots, \bar{p} - 1$ and by

$$\psi_1(\lambda) = \frac{\lambda - \lambda_2}{\lambda_1 - \lambda_2} I_{[\lambda_1, \lambda_2]}(\lambda) \tag{9b}$$

$$\psi_{\bar{p}}(\lambda) = \frac{\lambda - \lambda_{\bar{p}-1}}{\lambda_{\bar{p}} - \lambda_{\bar{p}-1}} I_{[\lambda_{\bar{p}-1}, \lambda_{\bar{p}}]}(\lambda) \tag{9c}$$

for $p = 1$ and $p = \bar{p}$. With $I_A(\cdot)$ we denote the indicator function of set A

$$I_A(x) = \begin{cases} 1, & \text{if } x \in A \\ 0, & \text{otherwise} \end{cases}. \tag{10}$$

The basis functions (9) are linear in each interval $[\lambda_l, \lambda_{l+1}]$ between the available parameter points. A similar definition is used for $\xi_q(\mu)$. The complete model expression including explicit dependence on all free variables reads

$$\mathbf{H}(s; \lambda, \mu) = \frac{\sum_{n,p,q} \mathbf{R}_{npq}\phi_n(s)\psi_p(\lambda)\xi_q(\mu)}{\sum_{n,p,q} r_{npq}\phi_n(s)\psi_p(\lambda)\xi_q(\mu)}. \tag{11}$$

[1] Throughout the paper, we will always denote the the minimum and maximum values taken by a quantity x as $\underline{x}$ and $\bar{x}$, respectively.

[2] In order to keep mathematical formulas reasonably compact, the lower and upper values of summation indexes will be often omitted. The lower value will be always 1 except for index n, that will start from 0 unless explicitly noted. The upper limit instead will always be the maximum value associated to the index (i.e., $\bar{n}$ for n, $\bar{p}$ for $p, \ldots$).

We remark that the order of numerator and denominator is the same, since the same basis poles are used. This is indeed the main enabling factor for the developments of Section IV, which will show how the basis poles cancel out in the final model expression. Note however that a different order for numerator and denominator polynomials is indeed possible. For example, one may want a numerator degree larger than denominator degree by one, in order to build macromodels with linear growth for large frequency (e.g., reproducing purely inductive or capacitive asymptotic behavior for impedance or admittance forms). This is easily achieved by adding $\phi_{-1}(s) = s$ to the set of numerator basis functions only. Therefore, without loss of generality, we will employ throughout the rest of this paper the same set of basis functions (7) for both numerator and denominator.

III. Parameterized Model Identification

A. Formulation

We present here an advanced identification procedure that allows estimation of the coefficients $\mathbf{R}_{npq}$ and r_{npq} in (11) from the raw data (4), while minimizing the modeling error

$$\mathcal{E}^2 = \sum_{l,m,k} \left\| \frac{\sum_n \mathbf{R}_n(\lambda_l,\mu_m)\phi_n(j\omega_k)}{\sum_n r_n(\lambda_l,\mu_m)\phi_n(j\omega_k)} - \mathbf{H}_{klm} \right\|_F^2 \tag{12}$$

where $\|\cdot\|_F$ denotes the Frobenius matrix norm.[3]

The numerical minimization of (12) poses two main challenges.

1) The identification problem is nonlinear, since some of the unknown coefficients appear at the denominator. This problem is common to all rational macromodeling algorithms, since the macromodel poles are never known *a priori*. Some good solutions are indeed possible, including the well-known vector fitting (VF) algorithm [3] and the iterative weighting process known as Sanathanan–Koerner iteration [2].
2) The number of free variables may grow very large. This number, which can be explicitly estimated and for the two-parameters case results $\bar{l}\bar{m}(\bar{n}+1)\times(N^2+1)$, grows exponentially with the number of parameters. The direct solution of (12) in a single step may therefore be unfeasible due to obvious complexity arguments.

These two challenges are here addressed using a smart formulation of the identification problem, which makes explicit use of the piecewise linear model structure. We will show in the following paragraphs that the proposed technique results in a great reduction of the overall computational cost for the identification, both in terms of CPU and memory requirements. In addition, it provides a much improved numerical accuracy and robustness with respect to other approaches.

Thanks to the piecewise-linear parameterization (8), the following interpolation property holds for the model coefficients

$$\mathbf{R}_n(\lambda_l,\mu_m) = \mathbf{R}_{nlm} \tag{13}$$

$$r_n(\lambda_l,\mu_m) = r_{nlm}. \tag{14}$$

[3]The Frobenius norm of a matrix $\mathbf{A}$ is given by $\|\mathbf{A}\|_F = \sqrt{\mathrm{Tr}(\mathbf{A}\mathbf{A}^H)}$ where Tr denotes the matrix trace and the superscript ^{H} the conjugate transpose.

Therefore, the model response $\mathbf{H}(s;\lambda_l,\mu_m)$ evaluated at the grid point (λ_l,μ_m) is only function of the few coefficients

$$\{\mathbf{R}_{nlm}\},\{r_{nlm}\},\quad n=0,\ldots,\bar{n} \tag{15}$$

with l and m fixed. Indeed, the modeling error can be written as sum of independent contributions $\mathcal{E}^2_{lm}$

$$\mathcal{E}^2 = \sum_{l=1}^{\bar{l}}\sum_{m=1}^{\bar{m}} \mathcal{E}^2_{lm} \tag{16}$$

where

$$\mathcal{E}^2_{lm} = \sum_{k=1}^{\bar{k}} \left\| \frac{\sum_n \mathbf{R}_{nlm}\phi_n(j\omega_k)}{\sum_n r_{nlm}\phi_n(j\omega_k)} - \mathbf{H}_{klm} \right\|_F^2. \tag{17}$$

Each factor $\mathcal{E}^2_{lm}$ represents the local modeling error at the grid point (λ_l,μ_m). Since these local errors are independent, i.e., they are functions of separate subsets of model coefficients, they can be independently minimized. If the minimum of (17) is achieved for each grid point (λ_l,μ_m), the global error (12) will be also minimized. This observation shows that the minimization of the fitting error (12) can be reformulated as $\bar{l}\bar{m}$ independent local minimum problems.

Minimization of (17) is a standard, non-parameterized fitting problem, that tries to match the frequency response $\mathbf{H}_{klm}$ (with l and m fixed)

$$\mathbf{H}_{lm}(j\omega_k) \simeq \mathbf{H}_{klm} \tag{18}$$

with the transfer function

$$\mathbf{H}_{lm}(s) = \frac{\sum_n \mathbf{R}_{nlm}\phi_n(s)}{\sum_n r_{nlm}\phi_n(s)}. \tag{19}$$

of a local, nonparameterized model. This reformulation of the original problem allows to use standard modeling algorithms to identify parameterized models in the form (6).

B. Fitting Algorithm

The independent local fitting problems (18) and (19) are not critical, and highly robust and efficient methods exist for their solution. The VF algorithm [3] is probably the best choice and will be used here. This method produces a macromodel in poles/residues form using an iterative poles relocation procedure, which is well-documented in the literature. When applied to the raw data $\mathbf{H}_{klm}$ with l and m fixed, it returns the individual model

$$\mathbf{H}_{lm}(s) = \mathbf{Q}_{0lm} + \sum_{n=1}^{\bar{n}} \frac{\mathbf{Q}_{nlm}}{s - p_{nlm}} \tag{20}$$

where $\mathbf{Q}_{nlm}$ and p_{nlm} are respectively the model residues and poles, with $\mathbf{Q}_{0lm}$ being the direct coupling constant.

If the above local identification process is applied to each independent grid point (λ_l,μ_m), the resulting sets of macromodel poles

$$\mathcal{P}_{lm} = \{p_{nlm},\ n=1,\ldots,\bar{n}\} \tag{21}$$

have no relation with each other. It is well known that model poles are very sensitive quantities to even small variations

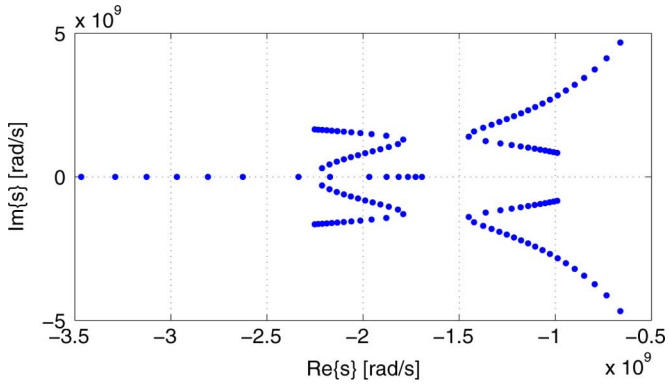

Fig. 1. Sketch of poles location of a fourth-order circuit with varying components. Bifurcation effects show that a direct parameterization of the model poles is nonsmooth and should be avoided.

of the parameters. Bifurcation effects may occur, resulting in quite irregular variations of each pole in the parameters space. See Fig. 1 for a graphical illustration on a simple test case. In addition, the poles/residues form (20) is not fully compatible with the model representation (6), which is based on a set of frequency-domain expansion functions $\{\phi_n(s)\}$, which are defined on a different but common set of poles $\{a_n\}$.

Fortunately, there is a full compatibility between (20) and (19), since a direct conversion can be performed from one format to the other, and vice-versa. Here, we are interested in converting (20) into (19). The following theorem provides the conversion rules for the computation of global coefficients $\mathbf{R}_{nlm}$ and r_{nlm} from local coefficients $\mathbf{Q}_{nlm}$ and p_{nlm}.

Theorem 1: Under the hypothesis that the poles $\{a_n\}$ are distinct, the transfer functions

$$\mathbf{H}_1(s) = \mathbf{Q}_0 + \sum_{n=1}^{\bar{n}} \frac{\mathbf{Q}_n}{s - p_n} \tag{22}$$

and

$$\mathbf{H}_2(s) = \frac{\mathbf{R}_0 + \sum_{n=1}^{\bar{n}} \frac{\mathbf{R}_n}{s-a_n}}{r_0 + \sum_{n=1}^{\bar{n}} \frac{r_n}{s-a_n}} \tag{23}$$

are equal if

$$\sum_{n=1}^{\bar{n}} r_n \prod_{\substack{n'=1 \\ n' \neq n}}^{\bar{n}} (p_l - a_{n'}) = -r_0 \prod_{n'=1}^{\bar{n}} (p_l - a_{n'}) \tag{24}$$

for $l = 1, \ldots, \bar{n}$,

$$\mathbf{R}_n = r_n \mathbf{H}_1(a_n) \tag{25}$$

for $n = 1, \ldots, \bar{n}$ and

$$\mathbf{R}_0 = r_0 \mathbf{Q}_0. \tag{26}$$

Proof: Let us rewrite (23) as ratio of two polynomials by multiplying numerator and denominator by $\prod_{n'=1}^{\bar{n}} (s - a_{n'})$

$$\mathbf{H}_2(s) = \frac{\mathbf{R}_0 \prod_{n'=1}^{\bar{n}} (s - a_{n'}) + \sum_{n=1}^{\bar{n}} \mathbf{R}_n \prod_{\substack{n'=1 \\ n' \neq n}}^{\bar{n}} (s - a_{n'})}{r_0 \prod_{n'=1}^{\bar{n}} (s - a_{n'}) + \sum_{n=1}^{\bar{n}} r_n \prod_{\substack{n'=1 \\ n' \neq n}}^{\bar{n}} (s - a_{n'})}. \tag{27}$$

To prove the first condition (24) we force the poles of (27) to equal the poles of (22) by setting to zero the denominator of (27) for $s = p_l$, with $l = 1, \ldots, \bar{n}$

$$r_0 \prod_{n'=1}^{\bar{n}} (p_l - a_{n'}) + \sum_{n=1}^{\bar{n}} r_n \prod_{\substack{n'=1 \\ n' \neq n}}^{\bar{n}} (p_l - a_{n'}) = 0. \tag{28}$$

This condition allows to compute the denominator coefficients $\{r_n\}$ of (23) with the solution of a linear system. Since there is a degree-of-freedom in the coefficients of (23), the value of r_0 can be fixed at will. The second condition (25) is obtained by evaluating $\mathbf{H}_2(s) = \mathbf{H}_1(s)$ for $s = a_n$, $n = 1, \ldots, \bar{n}$, and from the fact that $\mathbf{H}_2(a_n) = \mathbf{R}_n / r_n$, as evident from (27). Finally, condition (26) follows by imposing $\mathbf{H}_1(s) = \mathbf{H}_2(s)$ for $s \to \infty$.

The solution of linear system (24), followed by a direct evaluation of (25) and (26) for each grid point (λ_l, μ_m) provides the full set of coefficients $\mathbf{R}_{nlm}$ and r_{nlm} defining the proposed parameterized macromodel (6), starting from the collective set of independent poles and residues obtained by local fitting (19) at individual grid points.

C. Choice of Basis Poles

We discuss now the choice of basis poles $\{a_n\}$. We start noting that these poles are not used in the first stage of the fitting algorithm, the identification of the local models (20), which is performed using standard VF. Their choice has therefore no effects on this task. Basis poles come into play later, when all local models (20) are expressed with respect to the common basis $\phi_n(s)$ adopted for the final parametric model. The choice of basis poles a_n should be done in order to optimize the numerical conditioning of basis functions $\phi_n(s)$, in order to ease the conversion from the VF form (20) to (19). It is well known that the proposed rational basis (7) is well conditioned if the basis poles a_n are linearly distributed over the available bandwidth [3]. Therefore, we adopt this rule to displace the basis poles a_n.

To further support this conclusion we devised the following numerical test on the application example of Section VI-B. We computed the condition number of the linear system to be solved in the model conversion (24) for several displacements of the basis poles a_n.

- Linear: Linear displacement over the available bandwidth suggested in [3].
- Response poles: The basis poles $\{a_n\}$ are chosen as the poles of one of the available responses, estimated with standard VF.
- Linear, 10% bandwidth: Linear displacement over one tenth of the available bandwidth.
- Linear, 10× bandwidth: Linear displacement over ten times the available bandwidth.
- Linear with close poles: Linear displacement for all poles except for the first one, placed very close to the second pole $(a_1 = 0.99a_2)$.

Table I reports the numerical results of this test, and shows that the adopted rule (first case) provides the best conditioning of the model conversion formulas.

D. Stability Enforcement at Grid Points

Since VF guarantees the stability of the identified model, the final parameterized model (6) will be stable by construction at all grid points (λ_l, μ_m). It is clear that this stability enforcement process does not guarantee uniform stability of (6) at each point in the parameters space (5). However, it strongly reduces the occurrence of stability violations, and can be used to guarantee stability in the whole parameters range. In fact, if the model turns out to be unstable in a certain region, the interpolation grid can be there refined by adding more interpolation points where stability is preserved by construction, until uniform stability is achieved. In case of multiple parameters, those that produce the most relevant variations of the system response should be refined first, since stability violations are unlikely where variations due to parameters are small. By adding more samples with respect to these most critical parameters, the cause of stability loss is removed and the probability of obtaining uniform stability is maximized.

Such a procedure clearly needs for a reliable algorithm to test uniform stability and localize possible violations. This need motivates the developments of Section V, where we present a robust numerical algorithm for checking the uniform stability of parameterized models in the form (6), without resorting to brute-force sampling methods, which are slow and possibly misleading. Before presenting such testing procedures, we need to further elaborate on the model realization.

IV. Model Realization

In this section, a state-space realization of the parameterized model transfer function (6) is first derived, and then converted to a descriptor form. This form is very convenient, since it allows the construction of a uniform stability test for the parameterized macromodel (6). A brief review of the main definition and properties of descriptor systems is available in Appendix A.

A. State-Space Realization

In the following derivations, we will adopt the standard notation for state-space realizations:

$$\mathbf{H}(s) = \mathbf{D} + \mathbf{C}(s\mathbf{I} - \mathbf{A})^{-1}\mathbf{B} \leftrightarrow \left[\begin{array}{c|c} \mathbf{A} & \mathbf{B} \\ \hline \mathbf{C} & \mathbf{D} \end{array}\right]. \tag{29}$$

A state-space realization for (6) can be obtained if the model transfer function is interpreted as the ratio of two transfer functions $\mathbf{H}_1(s, \lambda, \mu)$ and $H_2(s, \lambda, \mu)$

$$\mathbf{H}(s; \lambda, \mu) = \frac{\mathbf{H}_1(s; \lambda, \mu)}{H_2(s; \lambda, \mu)} \tag{30}$$

where

$$\mathbf{H}_1(s; \lambda, \mu) = \mathbf{R}_0(\lambda, \mu) + \sum_{n=1}^{\bar{n}} \frac{\mathbf{R}_n(\lambda, \mu)}{s - a_n} \tag{31}$$

$$H_2(s; \lambda, \mu) = r_0(\lambda, \mu) + \sum_{n=1}^{\bar{n}} \frac{r_n(\lambda, \mu)}{s - a_n}. \tag{32}$$

First, we construct two separate state-space realizations for the numerator and denominator. We have

$$\mathbf{H}_1(s; \lambda, \mu) \leftrightarrow \left[\begin{array}{c|c} \mathbf{A}_1 & \mathbf{B}_1 \\ \hline \mathbf{C}_1(\lambda, \mu) & \mathbf{D}_1(\lambda, \mu) \end{array}\right] \tag{33}$$

$$H_2(s; \lambda, \mu)\mathbf{I}_N \leftrightarrow \left[\begin{array}{c|c} \mathbf{A}_2 & \mathbf{B}_2 \\ \hline \mathbf{C}_2(\lambda, \mu) & \mathbf{D}_2(\lambda, \mu) \end{array}\right] \tag{34}$$

where

- $\mathbf{A}_1 = \mathbf{A}_2 = \text{blkdiag}\{a_n \mathbf{I}_N\}$ with $n = 1, \ldots, \bar{n}$;
- $\mathbf{B}_1 = \mathbf{B}_2 = [\mathbf{I}_N, \ldots, \mathbf{I}_N]^T$ is a block-column matrix obtained by stacking $\bar{n}$ identity matrices;
- $\mathbf{C}_1(\lambda, \mu) = [\mathbf{R}_1(\lambda, \mu), \ldots, \mathbf{R}_{\bar{n}}(\lambda, \mu)]$;
- $\mathbf{C}_2(\lambda, \mu) = [r_1(\lambda, \mu)\mathbf{I}_N, \ldots, r_{\bar{n}}(\lambda, \mu)\mathbf{I}_N]$;
- $\mathbf{D}_1(\lambda, \mu) = \mathbf{R}_0(\lambda, \mu)$;
- $\mathbf{D}_2(\lambda, \mu) = r_0(\lambda, \mu)\mathbf{I}_N$.

We remark that, in case of complex poles $\{a_n\}$, the above state-space matrices are complex. However, standard coordinate changes can be applied in the state space such that the realization is real [23]. Henceforth, we will sometimes omit the dependence of the matrices $\mathbf{C}_1, \mathbf{C}_2, \mathbf{D}_1$, and $\mathbf{D}_2$ from λ and μ, in order to avoid formulas of excessive length.

Although the denominator function is scalar, its realization has been chosen to have N ports, in order to be compatible in size with the realization of the numerator. Then, a realization for the inverse of $H_2(s; \lambda, \mu)$ is derived from (34)

$$H_2^{-1}(s; \lambda, \mu)\mathbf{I}_N \leftrightarrow \left[\begin{array}{c|c} \mathbf{A}_2 - \mathbf{B}_2\mathbf{D}_2{}^{-1}\mathbf{C}_2 & -\mathbf{B}_2\mathbf{D}_2{}^{-1} \\ \hline \mathbf{D}_2{}^{-1}\mathbf{C}_2 & \mathbf{D}_2{}^{-1} \end{array}\right] \tag{35}$$

using standard manipulations, see [24] for details. Finally, $\mathbf{H}(s; \lambda, \mu)$ is realized by cascading (33) and (35) as

$$\begin{aligned} \mathbf{H}(s; \lambda, \mu) &= \mathbf{H}_1(s; \lambda, \mu) H_2^{-1}(s; \lambda, \mu)\mathbf{I}_N \\ &\leftrightarrow \left[\begin{array}{cc|c} \mathbf{A}_1 & \mathbf{B}_1\mathbf{D}_2{}^{-1}\mathbf{C}_2 & \mathbf{B}_1\mathbf{D}_2{}^{-1} \\ \mathbf{0} & \mathbf{A}_2 - \mathbf{B}_2\mathbf{D}_2{}^{-1}\mathbf{C}_2 & -\mathbf{B}_2\mathbf{D}_2{}^{-1} \\ \hline \mathbf{C}_1 & \mathbf{D}_1\mathbf{D}_2{}^{-1}\mathbf{C}_2 & \mathbf{D}_1\mathbf{D}_2{}^{-1} \end{array}\right]. \end{aligned} \tag{36}$$

B. Reduction of the Number of States

The number of state variables in (36) is $2N\bar{n}$, at least twice as large than necessary. In fact, it can be easily seen that $N\bar{n}$ states are not controllable and do not contribute to the input-output transfer function. This is evident if one considers that the poles of (36) are equal to[4]

$$\begin{aligned} &\text{eig}\{\mathbf{A}_1\} \cup \text{eig}\{\mathbf{A}_2 - \mathbf{B}_2\mathbf{D}_2{}^{-1}(\lambda, \mu)\mathbf{C}_2(\lambda, \mu)\} \\ &\quad = \{a_n\} \cup \text{eig}\{\mathbf{A}_2 - \mathbf{B}_2\mathbf{D}_2{}^{-1}(\lambda, \mu)\mathbf{C}_2(\lambda, \mu)\} \end{aligned} \tag{37}$$

while the poles of the original transfer function (6) are only $\text{eig}\{\mathbf{A}_2 - \mathbf{B}_2\mathbf{D}_2{}^{-1}(\lambda, \mu)\mathbf{C}_2(\lambda, \mu)\}$, i.e., the zeros of $H_2(s; \lambda, \mu)$. Indeed, the poles $\{a_n\}$ cancel out since they are common to the numerator and the denominator of (6).

The redundant states can be removed if (36) is cast to the Kalman controllable canonical form [24] with the similarity transformation

[4]Note that the poles $\{a_n\}$ of $\mathbf{A}_1$ are multiple.

TABLE I
CONDITION NUMBER OF THE LINEAR SYSTEM OF (24) FOR DIFFERENT DISPLACEMENTS OF BASIS POLES $\{a_n\}$. RF DEVICE OF SECTION IV-B IS CONSIDERED. MINIMUM AND MAXIMUM VALUES OBSERVED IN THE CONVERSION OF THE DIFFERENT LOCAL MODELS ARE REPORTED

Displacement	Conditioning of (24) [min,max]
Linear	$[5\times10^{6}, 3\times10^{7}]$
Response poles	$[6\times10^{6}, 3\times10^{7}]$
Linear, 10% bandwidth	$[1\times10^{10}, 5\times10^{10}]$
Linear, 10x bandwidth	$[2\times10^{7}, 3\times10^{7}]$
Linear with close poles	$[2\times10^{8}, 1\times10^{9}]$

$$\boldsymbol{x}(t;\lambda,\mu) = \mathbf{T}\boldsymbol{w}(t;\lambda,\mu) \tag{38}$$

where $\boldsymbol{x}(t;\lambda,\mu)$ denotes the state vector of (36), $\boldsymbol{w}(t;\lambda,\mu)$ is the new state vector in a different coordinate system, and the corresponding transformation matrix reads

$$\mathbf{T} = \frac{1}{\sqrt{2}}\begin{bmatrix} \mathbf{I} & \mathbf{I} \\ -\mathbf{I} & \mathbf{I} \end{bmatrix} \tag{39}$$

with $\mathbf{I}$ being the identity matrix of size $N\bar{n}\times N\bar{n}$. Application of (38) to (36) leads, after removal of the uncontrollable states, to the more compact realization

$$\mathbf{H}(s;\lambda,\mu) \leftrightarrow \left[\begin{array}{c|c} \mathbf{A_2} - \mathbf{B_2}\mathbf{D_2}^{-1}\mathbf{C_2} & \mathbf{B_2}\mathbf{D_2}^{-1} \\ \hline \mathbf{C_1} - \mathbf{D_1}\mathbf{D_2}^{-1}\mathbf{C_2} & \mathbf{D_1}\mathbf{D_2}^{-1} \end{array}\right]. \tag{40}$$

C. Descriptor Form

The realization (40) does not depend linearly on the matrices $\mathbf{C}_1(\lambda,\mu)$, $\mathbf{C}_2(\lambda,\mu)$, $\mathbf{D}_1(\lambda,\mu)$, $\mathbf{D}_2(\lambda,\mu)$ which are functions of the parameters λ and μ. We now show that a much simpler realization can be constructed such that linearity is preserved. This constraint will require to adopt a slightly more general form of realization, namely a so-called descriptor form, also known as a differential-algebraic system of equations (DAE) or, in circuit notation, as a modified nodal analysis (MNA) system. See Appendix A for details. A few straightforward manipulations show that the following descriptor system

$$\mathbf{E}\dot{\boldsymbol{x}}(t;\lambda,\mu) = \mathbf{A}(\lambda,\mu)\boldsymbol{x}(t;\lambda,\mu) + \mathbf{B}\boldsymbol{u}(t) \tag{41a}$$
$$\boldsymbol{y}(t;\lambda,\mu) = \mathbf{C}(\lambda,\mu)\boldsymbol{x}(t;\lambda,\mu) \tag{41b}$$

with

$$\mathbf{E} = \begin{bmatrix} \mathbf{I} & \mathbf{0} \\ \mathbf{0} & \mathbf{0} \end{bmatrix} \quad \mathbf{A}(\lambda,\mu) = \begin{bmatrix} \mathbf{A_2} & \mathbf{B_2} \\ \mathbf{C}_2(\lambda,\mu) & \mathbf{D}_2(\lambda,\mu) \end{bmatrix} \tag{42a}$$

$$\mathbf{B} = \begin{bmatrix} \mathbf{0} \\ -\mathbf{I}_N \end{bmatrix} \quad \mathbf{C}(\lambda,\mu) = \begin{bmatrix} \mathbf{C}_1(\lambda,\mu) & \mathbf{D}_1(\lambda,\mu) \end{bmatrix} \tag{42b}$$

is equivalent to the realization (40). It is evident that all blocks of this representation depend linearly on the parameter-dependent matrices $\mathbf{C}_1(\lambda,\mu)$, $\mathbf{C}_2(\lambda,\mu)$, $\mathbf{D}_1(\lambda,\mu)$, $\mathbf{D}_2(\lambda,\mu)$. Therefore, this formulation inherits the piecewise linear parameterization scheme introduced for the model coefficients (8). It is also remarkable that a large part of this system (the first $N\bar{n}$ equations) does not depend on the parameters. The above piecewise linear nature of the parameterized descriptor form is essential for the development of the uniform stability check, to be introduced in next Section.

V. UNIFORM STABILITY ASSESSMENT

In this section, we present a purely algebraic method for checking the stability of parameterized models uniformly with respect to the parameters λ and μ. The devised procedure is based on the descriptor form realization (41), since its matrices have a very simple dependence on the parameters.

A. Polytopic Nature of the Model Matrices

Starting from (42a) and (42b), it can be easily seen that both $\mathbf{A}(\lambda,\mu)$ and $\mathbf{C}(\lambda,\mu)$ are piecewise linear functions of λ and μ and can be expressed as

$$\mathbf{A}(\lambda,\mu) = \sum_{p=1}^{\bar{p}}\sum_{q=1}^{\bar{q}} \mathbf{A}_{pq}\psi_p(\lambda)\xi_q(\mu) \tag{43}$$

with

$$\mathbf{A}_{pq} = \begin{bmatrix} & \mathbf{A_2} & \\ r_{1pq}\mathbf{I}_N & \cdots & r_{\bar{n}pq}\mathbf{I}_N \end{bmatrix} \quad \begin{matrix} \mathbf{B_2} \\ r_{0pq}\mathbf{I}_N \end{matrix} \tag{44}$$

and

$$\mathbf{C}(\lambda,\mu) = \sum_{p=1}^{\bar{p}}\sum_{q=1}^{\bar{q}} \mathbf{C}_{pq}\psi_p(\lambda)\xi_q(\mu) \tag{45}$$

with

$$\mathbf{C}_{pq} = [\,\mathbf{R}_{1pq} \quad \cdots \quad \mathbf{R}_{\bar{n}pq} \qquad \mathbf{R}_{0pq}\,]. \tag{46}$$

Therefore, for each rectangular subdomain

$$(\lambda,\mu) \in [\lambda_l, \lambda_{l+1}] \times [\mu_m, \mu_{m+1}] \tag{47}$$

of the parameters space, the system matrices (42a) and (42b) are either multiaffine[5] in the parameters or constant. In fact, $\mathbf{A}(\lambda,\mu)$ and $\mathbf{C}(\lambda,\mu)$ can be written in the subdomain (47) as

$$\begin{aligned}\mathbf{A}(\lambda,\mu) = {} & \mathbf{A}_{lm}(1-\lambda')(1-\mu') + \mathbf{A}_{l+1,m}\lambda'(1-\mu') \\ & + \mathbf{A}_{l,m+1}(1-\lambda')\mu' + \mathbf{A}_{l+1,m+1}\lambda'\mu'\end{aligned} \tag{48}$$

$$\begin{aligned}\mathbf{C}(\lambda,\mu) = {} & \mathbf{C}_{lm}(1-\lambda')(1-\mu') + \mathbf{C}_{l+1,m}\lambda'(1-\mu') \\ & + \mathbf{C}_{l,m+1}(1-\lambda')\mu' + \mathbf{C}_{l+1,m+1}\lambda'\mu'\end{aligned} \tag{49}$$

where

$$\lambda' = \frac{\lambda-\lambda_l}{\lambda_{l+1}-\lambda_l} \qquad \mu' = \frac{\mu-\mu_m}{\mu_{m+1}-\mu_m}. \tag{50}$$

Expressions (48) and (49) show that, within each rectangle (47), $\mathbf{A}(\lambda,\mu)$ and $\mathbf{C}(\lambda,\mu)$ take values in the convex hull identified by the "corner" matrixes

[5]A function is multiaffine in its arguments if it is linear (affine) in each argument. Multiaffine functions are also called bilinear functions.

$$\begin{bmatrix}\mathbf{A}(\lambda,\mu)\\ \mathbf{C}(\lambda,\mu)\end{bmatrix} \in \mathrm{Co}\left\{\begin{bmatrix}\mathbf{A}_{lm}\\ \mathbf{C}_{lm}\end{bmatrix}, \begin{bmatrix}\mathbf{A}_{l+1,m}\\ \mathbf{C}_{l+1,m}\end{bmatrix}, \begin{bmatrix}\mathbf{A}_{l,m+1}\\ \mathbf{C}_{l,m+1}\end{bmatrix}, \begin{bmatrix}\mathbf{A}_{l+1,m+1}\\ \mathbf{C}_{l+1,m+1}\end{bmatrix}\right\}. \quad (51)$$

Therefore, the system matrices belong to a so-called convex polytopic domain. For this kind of systems, conditions for uniform stability can be found in the robust control literature [25]. These conditions, which involve the feasibility of certain linear matrix inequalities (LMI), are reviewed in the following. The reader is referred to [26], [27] for general concepts about LMIs and their numerical solution.

B. Uniform Stability

We now consider testing the uniform stability of proposed macromodels. We have the following result [25], which we report without proof.

Theorem 2: The system (41) is admissible (i.e., stable, regular and impulse-free, see Appendix A) for all parameter values in the subdomain (47) if there exist two matrices $\mathbf{P} = \mathbf{P}^T > 0$ and $\mathbf{Q}$ such that the following set of LMIs holds

$$(\mathbf{P}\mathbf{E}^T + \mathbf{S}\mathbf{Q})^T \mathbf{A}_{pq}^T + \mathbf{A}_{pq}(\mathbf{P}\mathbf{E}^T + \mathbf{S}\mathbf{Q}) < 0 \quad (52)$$

with $p = l, l+1$, $q = m, m+1$, and where $\mathbf{S} \in \mathbb{R}^{N(\bar{n}+1)\times N}$ is any matrix with full column rank that satisfies $\mathbf{E}\mathbf{S} = 0$. The specific choice of matrix $\mathbf{S}$ provides extra degrees-of-freedom for tuning the performance of the LMI solver. In our case, we can choose the explicit form $\mathbf{S} = [\,0\,\mathbf{I}_N\,]^T$, which provides the simplest expression fulfilling the hypothesis of Theorem 2.

A few comments are in order. It is easily recognized that the LMI condition (52) collects a set of Lyapunov stability equations, each corresponding to a "corner" model, extracted from (41), for the subdomain (47). The theorem states that when these Lyapunov equations hold simultaneously with common matrices $\mathbf{P}$ and $\mathbf{Q}$, then the model is uniformly stable in the entire subdomain (47). This condition is very powerful, since only a feasibility check of LMI condition (52) is required. This operation can be performed with standard convex programming methods [27] in a finite number of steps. In this work, we use the well-known SeDuMi solver [28]. We remark that this procedure avoids possibly unreliable and time consuming brute-force dense sampling in the parameters space, that have to scan the whole space to ascertain model stability.

The uniform stability conditions set by Theorem 2 are sufficient but not necessary. Therefore, if these conditions do not hold in a certain subdomain (47), one cannot conclude that there is a stability violation for sure. In this case, one can adopt the following strategy to find stability violations. First, the subdomain (47) is further divided into smaller rectangles, where Theorem 2 is applied in order to detect areas where (6) is surely stable. Then, if stability is still unknown in some of these small areas, a local sampling can be there performed to localize possible stability violations. We remark that this resort to sampling does not significantly affect the computational cost of the proposed uniform stability test. If fact, sampling is only applied in some small zones, where a few check points are sufficient. Moreover, since model is likely to be unstable in these areas, only a few check points must be scanned to find a stability violation and stop the sweep since the model instability has been proved.

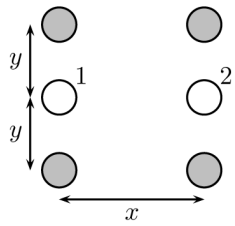

Fig. 2. Cross section of the transmission line example. Signal lines are numbered; reference conductors are grayed.

VI. Application Examples

A. Coupled Wires With Variable Separation

We consider a multiconductor transmission line composed by six parallel wires; the conductors are 2 cm long and have a diameter of 1 mm. The cross section is depicted in Fig. 2 and depends on the two free variables x and y, which represent the horizontal and vertical spacing between the conductors. The two inner conductors are the signal lines, while the other four act as reference. This example reproduces the simplified geometry of a high-speed connector, with varying horizontal and vertical pitch.

The purpose of this example is twofold. First, we want to test the algorithm accuracy on this four-port structure that exhibits both large and small S parameters, being the transmission coefficients and the lines crosstalk. Second, this structure will show on a practical example the low computational complexity of the proposed approach, which allows the quick identification of a two-parameters model for the whole four-port structure.

The scattering parameters of the line were computed up to 20 GHz for several values of the two design parameters. The horizontal spacing x was swept between 3.5 and 4.5 mm at steps of 0.1 mm. The vertical spacing from 2.5 up to 3.5 mm with the same 0.1-mm step. Out of these responses, those for $x \in \{3.5, 3.7, 3.9, 4.1, 4.3, 4.5\}$ mm and $y \in \{2.5, 2.7, 2.9, 3.1, 3.3, 3.5\}$ mm were used to identify a parameterized macromodel, as a multivariate function of frequency, x and y. The other responses were instead used as a validation set, in order to assess the model quality in the whole parameters range once the identification was completed.

A parameterized model of order 16 was identified for the entire four-port structure. The maximum modeling error turned out to be 9.3×10^{-3} on the fitting responses and 9.7×10^{-3} on the validation responses. The modeling error for all available configurations of x and y is shown in Fig. 4. Fig. 3 further demonstrates the excellent accuracy of the computed macromodel, which is able to precisely reproduce the weak far-end crosstalk $\mathbf{S}_{14}$ between the two signal lines. Thanks to the low computational complexity of the proposed algorithm, the identification of the four-port multivariate model took only 19 s on a 1.8-GHz laptop with 1.5 GB of memory. This is a quite remarkable result, especially if one considers that previously published techniques [20], [21], would have required about 2 GB of

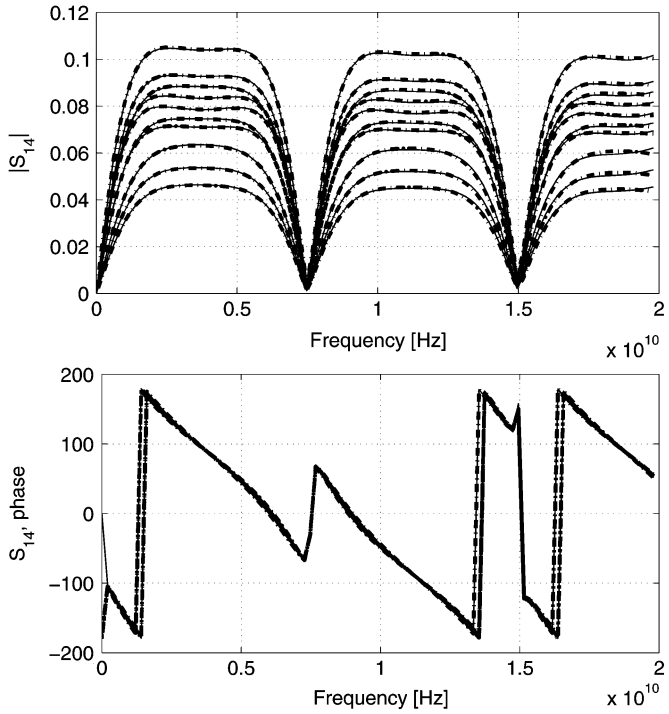

Fig. 3. Far end crosstalk $\mathbf{S}_{14}$ for the coupled lines of Fig. 2. The model response (dash-dot line) is compared with the original data (solid line) for (x, y) equal to the worst case configuration (3.6,2.5) mm, and the parameters configurations (4,2.5), (4.4,2.5), (3.8,2.9), (3.5,3), (4.2,3.1), (3.6,3.2), (3.5,3.4), (4.1,3.4), (4.4,3.5) mm.

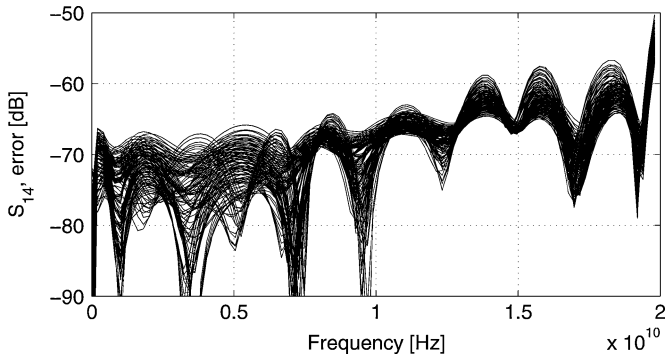

Fig. 4. Modeling error for the far-end crosstalk $\mathbf{S}_{14}$ for all available combinations of parameters x and y.

memory just to allocate the matrix associated with the fitting equations.

The uniform stability of the model in the parameters range was assessed with the LMI based algorithm proposed in Section V-B. In all subdomains (47) the model turned out to be uniformly stable, as further confirmed by Fig. 5, where the model poles are depicted for several values of the parameters. A brute-force stability test was also performed by sweeping the two parameters in (5) at steps of 0.02 mm. Model stability was confirmed also by this test, that however is less accurate than the LMI-based test and more time consuming. For this example, the algorithm devised in Section V-B took only 63 s, while the brute force check took more than 5 minutes.

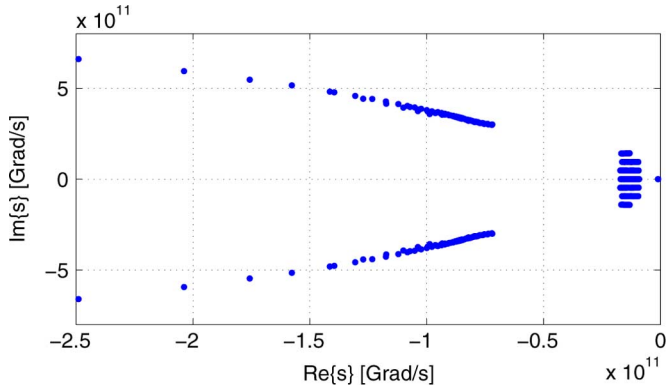

Fig. 5. Model poles as a function of the parameters x and y.

TABLE II
PORTS DESCRIPTION FOR THE RF DEVICE OF SECTION VI-B

Port	Description
1,2	Differential input
3,4	Differential output
5	Block enable/disable
6	Power supply (high)
7	Power supply (low)

B. RF Circuit Block

As a second example we consider a seven-ports RF circuit block located in several multimode GSM and EDGE transceivers for wireless applications and built in 130 nm CMOS technology (courtesy of Dr. P. Brenner, Infineon Technologies AG). A brief description of the circuitry ports is provided in Table II. The small-signal scattering matrix depends on the bias level V_B, which is a free parameter ranging from 0.15 V up to 1 V. The device exhibits a strong nonlinear behavior with respect to the V_B parameter and is thus a good benchmark for the presented technique.

In order to construct a bias-dependent parameterized macromodel, the scattering parameters of the linearized device were computed from 0 up to 40 GHz for increasing bias values V_B in 25 mV steps. An additional set of responses for intermediate values of V_B was then used to validate the model quality after identification.

Fig. 6 compares the transmission coefficient $\mathbf{S}_{31}$ of a parameterized model of order 6 with the original data, for the validation values of V_B. An excellent match between the model behavior and the reference data can be observed, even if the model response changes quite rapidly, as can be observed in Fig. 7, where the magnitude of the macromodel $\mathbf{S}_{31}$ parameter is depicted versus frequency and V_B. The computed model turned out to be very accurate on all 49 elements of the S matrix, with a maximum error between the model and the validation data of 3.2×10^{-3}. In Fig. 8 the reflection coefficient at port 4 of the model is shown versus frequency and parameter V_B. With the proposed technique, the model was identified in only 6 s, since standard VF was applied sequentially to the different responses, minimizing both computational cost and memory consumption, that was negligible. This result represents a major improvement with respect to earlier works on parametric macromodeling [20], [21] that in this case would require the solution of some fully

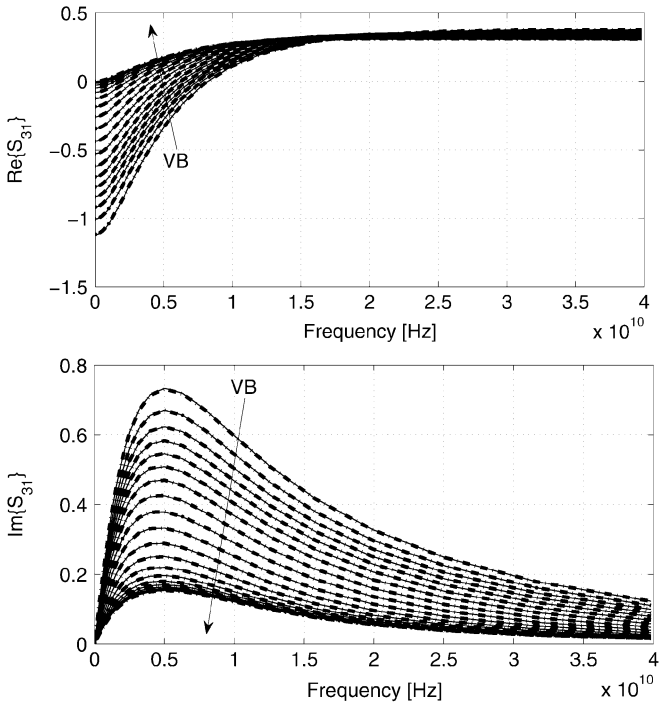

Fig. 6. Real (top) and imaginary (bottom) part of the $\mathbf{S}_{31}$ transmission coefficients of the RF device. Solid lines represent the original data, dash-dot lines the parametric model response.

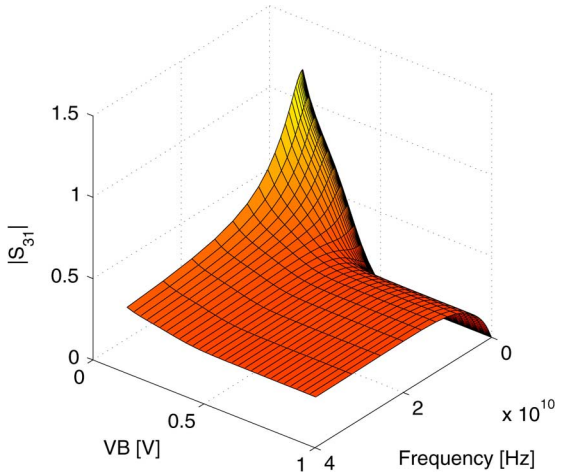

Fig. 7. Magnitude of $\mathbf{S}_{31}$ of the parametric model, versus frequency and V_B.

coupled least squares problems with about 230 000 constraints and more than 700 unknowns, for a memory consumption larger than 1.3 GB.

Finally, application of the uniform stability check proposed in this paper showed that the computed model is stable uniformly over the whole parameter range $V_B \in [0.15, 1]V$.

VII. Conclusion

This paper proposed a new framework for the generation of parameterized macromodels. A new compact formulation is introduced for the accurate representation of broadband frequency and design parameters variations in a single multivariate macromodel expression. Then, an identification algorithm is presented, allowing for fast and reliable computation of the

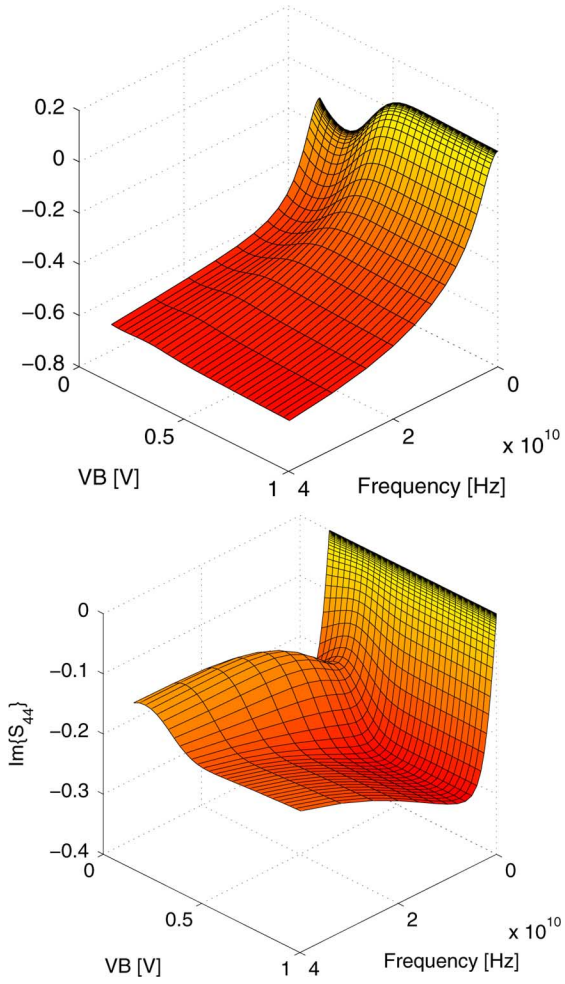

Fig. 8. Real (top panel) and imaginary (bottom panel) part of the $\mathbf{S}_{44}$ parameter for the RF device model.

model coefficients starting from a limited set of tabulated frequency responses. Finally, the macromodel is cast in a parameterized polytopic descriptor form. This formulation leads to a direct and simple method for checking its uniform stability over the entire range of parameters variation, based on a purely algebraic procedure that does not require dense sampling of the parameters space. The numerical examples show that the presented technique produces very accurate and reliable models, even for cases that are characterized by strong parameter-induced variations.

Appendix

A. Descriptor Systems

This appendix collects some important concepts on the descriptor representation of linear time-invariant systems used in the paper. The reader is referred to [25], [29], [30] for more details and for a comprehensive set of bibliographic references.

The descriptor form is a mathematical representation of singular systems, that generalizes the very popular state-space representation with the introduction of a matrix $\mathbf{E}$

$$\mathbf{E}\dot{\boldsymbol{x}}(t) = \mathbf{A}\boldsymbol{x}(t) + \mathbf{B}\boldsymbol{u}(t) \tag{53a}$$

$$\boldsymbol{y}(t) = \mathbf{C}\boldsymbol{x}(t) \tag{53b}$$

with $\boldsymbol{x}(t) \in \mathbb{R}^n$ and $\text{rank}\{\mathbf{E}\} = r$. In general $r < n$, so this representation supports singular systems governed by mixed dynamic and nondynamic (algebraic) equations, that do not fit in the state-space formalism. The transfer function $\mathbf{G}(s)$ of (53) is given by [25]

$$\mathbf{G}(s) = \mathbf{C}(s\mathbf{E} - \mathbf{A})^{-1}\mathbf{B} \tag{54}$$

with the poles being the generalized eigenvalues [31] of the matrix pencil $(\mathbf{E}, \mathbf{A})$

$$\rho_i = \text{zeros}\{\det(s\mathbf{E} - \mathbf{A})\} \tag{55}$$

located both at finite and infinite frequency. The behavior of descriptor systems is therefore much richer than state-space systems, and is classified according to the following properties [25]:

- *regular* if $\det(s\mathbf{E} - \mathbf{A})$ is not identically vanishing;
- *impulse-free* if $\deg(\det(s\mathbf{E} - \mathbf{A})) = r$;
- *stable* if all poles ρ_i have negative real part;
- *admissible* if regular, impulse-free and stable.

The regularity property ensures the existence and uniqueness of the solution of (53) for any initial condition, while the impulse-free property the absence of impulsive modes [25].

ACKNOWLEDGMENT

The authors would like to thank Dr. P. Brenner of Infineon Technologies AG, Germany, for providing the RF device data used in one application example.

REFERENCES

[1] M. Nakhla and R. Achar, "Simulation of high-speed interconnects," *Proc. IEEE*, vol. 89, no. 5, pp. 693–728, May 2001.
[2] C. K. Sanathanan and J. Koerner, "Transfer function synthesis as a ratio of two complex polynomials," *IEEE Trans. Autom. Control*, vol. AC-9, no. 1, pp. 56–58, Jan, 1963.
[3] B. Gustavsen and A. Semlyen, "Rational approximation of frequency domain responses by vector fitting," *IEEE Trans. Power Del.*, vol. 14, no. 3, pp. 1052–1061, Jul. 1999.
[4] B. Gustavsen and A. Semlyen, "A robust approach for system identification in the frequency domain," *IEEE Trans. Power Del.*, vol. 19, no. 3, pp. 1167–1173, Jul. 2004.
[5] D. Deschrijver, B. Haegeman, and T. Dhaene, "Orthonormal vector fitting: A robust macromodeling tool for rational approximation of frequency domain responses," *IEEE Trans. Adv. Packag.*, vol. 30, no. 2, pp. 216–225, May 2007.
[6] S. Grivet-Talocia and M. Bandinu, "Improving the convergence of vector fitting in presence of noise," *IEEE Trans. Electromagn. Compatibil.*, vol. 48, no. 1, pp. 104–120, Feb. 2006.
[7] S. Grivet-Talocia, "Package macromodeling via time-domain vector fitting," *IEEE Microwave Wireless Comp. Lett.*, vol. 13, no. 11, pp. 472–474, Nov. 2003.
[8] IdEM 2.4. [Online]. Available: http://www.emc.polito.it
[9] W. Beyene and J. Schutt-Ainé, "Accurate frequency-domain modeling and efficient circuit simulation of high-speed packaging interconnects," *IEEE Trans. Microwave Theory Tech.*, vol. 45, no. 10, pp. 1941–1947, Oct. 1997.
[10] K. L. Choi and M. Swaminathan, "Development of model libraries for embedded passives using network synthesis," *IEEE Trans. Circuits Syst. II*, vol. 47, no. 4, pp. 249–260, Apr. 2000.
[11] W. Do Couto Boaventura, A. Semlyen, M. R. Iravani, and A. Lopes, "Sparse network equivalent based on time-domain fitting," *IEEE Trans. Power Del.*, vol. 17, no. 1, pp. 182–189, Jan. 2002.
[12] M. Elzinga, K. Virga, and J. L. Prince, "Improve global rational approximation macromodeling algorithm for networks characterized by frequency-sampled data," *IEEE Trans. Microwave Theory Tech.*, vol. 48, no. 9, pp. 1461–1467, Sep. 2000.
[13] P. Triverio, S. Grivet-Talocia, M. S. Nakhla, F. Canavero, and R. Achar, "Stability, causality, and passivity in electrical interconnect models," *IEEE Trans. Adv. Packag.*, vol. 30, no. 4, pp. 795–808, Nov. 2007.
[14] D. Saraswat, R. Achar, and M. Nakhla, "Global passivity enforcement algorithm for macromodels of interconnect subnetworks characterized by tabulated data," *IEEE Trans. Very Large Scale (VLSI) Syst.*, vol. 13, no. 7, pp. 819–832, Jul. 2005.
[15] C. P. Coelho, J. Phillips, and L. M. Silveira, "A convex programming approach for generating guaranteed passive approximations to tabulated frequency-data," *IEEE Trans. Computed-Aided Design Integr. Circuits Syst.*, vol. 23, no. 2, pp. 293–301, Feb. 2004.
[16] B. Gustavsen and A. Semlyen, "Enforcing passivity for admittance matrices approximated by rational functions," *IEEE Trans. Power Syst.*, vol. 16, no. 1, pp. 97–104, Feb. 2001.
[17] S. Grivet-Talocia, "Passivity enforcement via perturbation of Hamiltonian matrices," *IEEE Trans. Circuits Syst. I*, vol. 51, no. 9, pp. 1755–1769, Sep. 2004.
[18] S. Grivet-Talocia, "An adaptive sampling technique for passivity characterization and enforcement of large interconnect macromodels," *IEEE Trans. Adv. Packag.*, vol. 30, no. 2, pp. 226–237, May 2007.
[19] S. Grivet-Talocia, S. Acquadro, M. Bandinu, F. G. Canavero, I. Kelander, and M. Rouvala, "A parameterization scheme for lossy transmission line macromodels with application to high speed interconnects in mobile devices," *IEEE Trans. Electromagn. Compat.*, vol. 49, no. 1, pp. 18–24, Feb. 2007.
[20] P. Triverio, M. Nakhla, and S. Grivet-Talocia, "Parametric macromodeling of multiport networks from tabulated data," presented at the Topical Meeting Electrical Performance Electron. Packaging, Atlanta, GA, Oct. 29–31, 2007.
[21] P. Triverio, S. Grivet-Talocia, and M. Nakhla, "An improved fitting algorithm for parametric macromodeling from tabulated data," presented at the 12th Workshop Signal Propagation Interconnects (SPI 2008), Avignon, France, May 12–15, 2008.
[22] D. Deschrijver and T. Dhaene, "Parametric macromodeling of time domain responses," presented at the 12th Workshop Signal Propagation Interconnects (SPI 2008), Avignon, France, May 12–15, 2008.
[23] T. Kailath, *Linear Systems*. Englewood Cliffs, NJ: Prentice-Hall, 1980.
[24] K. Zhou, J. C. Doyle, and K. Glover, *Robust and Optimal Control*. Upper Saddle River, NJ: Prentice-Hall, 1996.
[25] S. Xu and J. Lam, *Robust Control and Filtering of Singular Systems*, ser. Lecture Notes in Control and Information Sciences. Berlin/Heidelberg, Germany: Springer, 2006, vol. 332.
[26] S. Boyd, L. El. Ghaoui, E. Feron, and V. Balakrishnan, *Linear Matrix Inequalities in System and Control Theory*, ser. Studies in Applied Mathematics. Philadelphia, PA: SIAM, 1994, vol. 15.
[27] S. Boyd and L. Vanderberghe, *Convex Optimization*. Cambridge, U.K.: Cambridge Univ. Press, 2004.
[28] J. F. Sturm, "Using SeDuMi 1.02, A MATLAB toolbox for optimization over symmetric cones," *Optimizat. Methods Software*, vol. 11–12, pp. 625–653, 1999.
[29] L. Dai, *Singular Control Systems*. New York: Springer-Verlag, 1989.
[30] F. L. Lewis, "A survey of linear singular systems," *Circuits Syst. Signal Process*, vol. 5, no. 1, pp. 3–36, 1986.
[31] F. R. Gantmacher, *Theory of Matrices*. Providence, RI: American Mathematical Society, 2000.

Piero Triverio (S'06) received the Laurea Specialistica degree (M.Sc.) in electronics engineering, in 2005, from the Polytechnic University of Turin, Turin, Italy, where he is currently working toward the Ph.D. degree in the Electromagnetic Compatibility Group.

In 2005 and 2007, he was visiting student with the Computer Aided Design Research Group at Carleton University, Ottawa, ON, Canada. His research interests are in the modeling and simulation of high-speed interconnects.

Mr. Triverio is co-recipient of the 2007 Best Paper Award of the IEEE TRANSACTIONS ON ADVANCED PACKAGING, and the recipient of the INTEL Best Student Paper Award presented at the IEEE 15th Topical Meeting on Electrical Performance of Electronic Packaging (EPEP 2006). He received the Optime Award of the Turin Industrial Association and in 2005 was selected for the IBM EMEA Top Student Recognition Event.

Stefano Grivet-Talocia (M'98–SM'07) received the Laurea and the Ph.D. degrees in electronic engineering from the Polytechnic University of Turin, Turin, Italy.

From 1994 to 1996, he was with the NASA/Goddard Space Flight Center, Greenbelt, MD, where he worked on applications of fractal geometry and wavelet transform to the analysis and processing of geophysical time series. Currently, he is an Associate Professor of Circuit Theory with the Department of Electronics, Polytechnic of Turin. His current research interests are in passive macromodeling of lumped and distributed interconnect structures, modeling and simulation of fields, circuits, and their interaction, wavelets, time-frequency transforms, and their applications. He is author of more than 90 journal and conference papers.

Dr. Grivet-Talocia is corecipient of the 2007 Best Paper Award of the IEEE TRANSACTIONS ON ADVANCED PACKAGING. He received the IBM Shared University Research (SUR) Award in 2007. He served as Associate Editor for the IEEE TRANSACTIONS ON ELECTROMAGNETIC COMPATIBILITY from 1999 to 2001.

Michel S. Nakhla (S'73–M'75–SM'88–F'98) received the M.A.Sc. and Ph.D. degrees in electrical engineering from University of Waterloo, Waterloo, ON, Canada, in 1973 and 1975, respectively.

He is a Chancellor's Professor of Electrical Engineering at Carleton University. From 1976 to 1988, he was with Bell-Northern Research, Ottawa, ON, Canada, as the Senior Manager of the Computer-Aided Engineering Group. In 1988, he joined Carleton University, Ottawa, ON, Canada as a Professor and the holder of the Computer-Aided Engineering Senior Industrial Chair established by Bell-Northern Research and the Natural Sciences and Engineering Research Council of Canada. He is the founder of the High-Speed CAD Research Group at Carleton University. He is serving on various international committees, including the standing committee of the IEEE International Signal Propagation on Interconnects Workshop (SPI), the technical program committee of the IEEE International Microwave Symposium (IMS), the technical program committee of the IEEE Topical Meeting on Electrical Performance of Electronic Packaging, and the CAD committee (MTT-1) of the IEEE Microwave Theory and Techniques Society. He serves as a technical consultant for several industrial organizations and is the principal investigator for several major sponsored research projects. His research interests include modeling and simulation of high-speed circuits and interconnects, nonlinear circuits, multidisciplinary optimization, thermal and electromagnetic emission analysis, MEMS and neural networks. He served as Associate Editor of the *Circuits, Systems and Signal Processing* journal. He has also served as a member of many Canadian and international government-sponsored research grants selection panels.

He is an Associate Editor of the IEEE TRANSACTIONS ON ADVANCED PACKAGING and served as Associate Editor of the IEEE TRANSACTIONS ON CIRCUITS AND SYSTEMS.